Carbohydrate Polymers 233 (2020) 115865

Contents lists available at ScienceDirect

Carbohydrate Polymers

journal homepage: www.elsevier.com/locate/carbpol

A surface functionalized with per-(6-amino-6-deoxy)-β-cyclodextrin for potential organic pollutant removal from water

Bárbara A. Herrera[a,b,*], Tamara C. Bruna[a], Rodrigo A. Sierpe[c], Erika P. Lang[d], Marcela Urzúa[a], Marcos I. Flores[e], Paul S. Jara[a,*], Nicolás I. Yutronic[a,*]

[a] Departamento de Química, Facultad de Ciencias, Universidad de Chile, Las Palmeras No 3425, Ñuñoa, CA. 7800003, Santiago, Chile
[b] Departamento de Química, Facultad de Ciencias Naturales, Matemática y Medio Ambiente, Universidad Tecnológica Metropolitana, Las Palmeras No 3360, Ñuñoa, CA. 7800003, Santiago, Chile
[c] Departamento de Toxicología y Farmacología, Facultad de Ciencias Químicas y Farmacéuticas, Universidad de Chile, Santos Dumont No 964, Independencia, CA. 8380494, Santiago, Chile
[d] Departamento de Biología, Centro de Equipamiento Mayor (CEM), Facultad de Ciencias, Universidad de Chile, Las Palmeras No 3425, Ñuñoa, CA. 7800003, Santiago, Chile
[e] Departamento de Física, Facultad de Ciencias Físicas y Matemáticas, Universidad de Chile, Av. Blanco Encalada No 2008, CA. 8370415 Santiago, Chile

ARTICLE INFO

Keywords:
Aminated β-cyclodextrin
Emerging pollutants
4-Chlorophenoxyacetic acid
Phenylethylamine
4-Aminobenzoic acid
Pollutant removal

ABSTRACT

In this work, we present a solid silicon substrate functionalized with modified β-cyclodextrin monolayers as an optimal surface for organic contaminant uptake. The inclusion and capture of three potential pollutants, 4-chlorophenoxyacetic acid, 4-aminobenzoic acid and phenylethylamine, were studied. ^{1}H-NMR and ROESY studies revealed the complete inclusion and details of the conformational orientation of the three guests in the per-(6-amino-6-deoxy)-β-cyclodextrin matrix, forming three new inclusion complexes that have not yet been reported. Capture assays for the guests were carried out by immersing the substrates in an aqueous pollutant solution and by measuring the UV–vis spectra. This substrate showed a high sorption capacity at equilibrium, between 2.5×10^{-5} and 6.0×10^{-5} mmol/substrate, for the studied pollutants. In addition, this surface can be reused four times with an efficiency equal to the initial use. Therefore, it could be a versatile platform that could be applied for the capture of other organic pollutants from water.

1. Introduction

Global pollutant accumulation, due to excessive use and/or incorrect handling, creates critical environmental damage (Awad et al., 2019; Ivshina, Tyumina, & Vikhareva, 2018). In this way, the preparation and evaluation of substrates capable of removing pollutants (e.g., organic herbicides, dyes, and drugs) is an area of interest for environmental research (Ahmad et al., 2010; Lu et al., 2019).

The pollutants present in water that can be classified according to their application or chemical nature. These include species that, because of their accumulation or recent unregulated use, are called emerging pollutants (Geissen et al., 2015). Chlorophenoxy pesticides are organic pollutants that can persist in the environment, contaminating surface water and groundwater due to their widespread use, resistance to biodegradation and moderate water solubility. The herbicide 4-chlorophenoxyacetic acid (4CPA) has higher water solubility compared to similar compounds in its class (Derylo-Marczewska, Blachnio, Marczewski, Swiatkowski, & Buczek, 2017; Leopold, van Schaik, & Neal, 1960).

Additionally, 4-aminobenzoic acid (4ABA) has been used for diazotization reactions in the synthesis of dyes and related applications such as dye degradation, which means that it may be an emerging pollutant (Naik et al., 2018; Wang, Zhao, Qian, & Huang, 2018). Phenylethylamine (PhEA) is an antidepressant and psychoactive stimulant that produces effects such as wakefulness, excitability and tachycardia. This drug can also be considered an emerging pollutant (Halberstadt, van der Zee, Chatha, Geyer, & Powell, 2019; Sabelli, Fink, Fawcett, & Tom, 1996; Sierpe et al., 2015).

An interesting strategy for capturing organic pollutants in water is the use of materials based on β-cyclodextrin (βCD) (Morin-Crini & Crini, 2013). Cyclodextrins are cyclic sugars obtained from enzymatic starch degradation (Del Valle, 2004). The hydrophobic character of the cavity and the hydrophilic character of the outside allow for the inclusion of organic and inorganic guest molecules within the cavity

* Corresponding authors.
E-mail addresses: bahi@ug.uchile.cl, herrera@utem.cl (B.A. Herrera), pjara@uchile.cl (P.S. Jara), nyutroni@uchile.cl (N.I. Yutronic).

https://doi.org/10.1016/j.carbpol.2020.115865
Received 4 June 2019; Received in revised form 16 December 2019; Accepted 12 January 2020
Available online 13 January 2020
0144-8617/

through intermolecular interactions (Crini, 2014; Del Valle, 2004). The internal diameter of native βCD is 7.5 Å (Crini, 2014), which is an adequate dimension for the inclusion of organic pollutant molecules that contain aromatic rings as well as aliphatic chains. βCD-based materials have been applied to remediate different organic pollutant molecules (Salazar, Guerra, Yutronic, & Jara, 2018; Schofield, Bain, & Badyal, 2012; Taka, Pillay, & Mbianda, 2017).

Assembled βCD monolayers (βCDMs) on surfaces represent an interesting research topic in areas such as analyte detection because they offer a unique way to confine molecules in two dimensions by controlling binding events at the interface (Lagrost, Alcaraz, Bergamini, Fabre, & Serbanescu, 2007; Lu et al., 2019; Méndez-Torres, Sandoval-Altamirano, Sánchez-Arenillas, Marco, & Yáñez, 2018; Pan et al., 2015). The arrangement of βCDMs can act as a template for molecular recognition where the matrix-guest intermolecular interactions are reversible, which means that βCDMs are able to include and release the guest molecules (Ling, Reinhoudt, & Huskens, 2008; Méndez-Torres et al., 2018; Niu et al., 2015; Onclin, Mulder, Huskens, Ravoo, & Reinhoudt, 2004).

Given the excellent properties of βCD in organic pollutant inclusion, in this work, we aimed to contribute to the study of materials useful in removing contaminating agents from wastewater. We modified a silicon surface with per-(6-amino-6-deoxy)-β-cyclodextrin ($\beta CDNH_2$) to study and evaluate its ability to capture organic pollutants from water, specifically an herbicide (4CPA), a dye precursor (4ABA) and a drug (PhEA).

2. Materials and methods

2.1. Reagents and solvents

For preparation of the inclusion complexes, per-(6-amino-6-deoxy)-β-CD hydrochloride ($\beta CDNH_2$, synthesized by our group, ≥98 % w/w; see Supplementary Material, S1), 4-chlorophenoxyacetic acid (4CPA, PESTANAL®, ≥98.0 % w/w; Sigma-Aldrich), phenylethylamine (PhEA, 99.5 % w/v; Sigma-Aldrich) and 4-aminobenzoic acid (4ABA > 99 % w/w; Merck) were used. The preparation of substrates modified with $\beta CDNH_2$ was performed using 3-aminopropyl triethoxysilane (APTES, ≥99 % w/v; Sigma-Aldrich), 1,4-phenylene diisothiocyanate (DITC, ≥98 % w/w; Sigma-Aldrich), toluene (LC grade; Merck), 25 % ammonia in water v/v solution (Merck), 30 % v/v hydrogen peroxide (Merck), and ultra-high purity water, which was purified using an SG-LaboStar 4-DI ultra-pure water system with a conductivity of 0.055 μS/cm. Silicon wafers (100) were purchased from Santa Clara, CA, USA. Deuterated water (D_2O, 99.9 % D atoms; Sigma-Aldrich) was used as the solvent for the NMR studies. Absolute ethanol (≥99.8 % w/v, GC grade; Sigma-Aldrich) was used as the solvent for the regeneration tests.

2.2. Formation of the inclusion complexes

The preparation of the inclusion complexes was performed in deuterated water using $\beta CDNH_2$ (7.0 $mmol L^{-1}$) as the matrix molecule and 4CPA, 4ABA and PhEA (7.0 $mmol L^{-1}$) as guests. Each inclusion complex was defined as $\beta CDNH_2$@4CPA, $\beta CDNH_2$@4ABA and $\beta CDNH_2$@PhEA, respectively.

2.3. Characterization by NMR

Inclusion complexes were characterized using proton nuclear magnetic resonance (^{1}H-NMR) spectroscopy and rotating-frame nuclear Overhauser effect (ROESY) spectroscopy (see Supplementary Material, S2). ^{1}H-NMR measurements were carried out at 300 K in D_2O using a Bruker Avance 400 MHz NMR spectrometer. ROESY spectra were acquired using pulsed field gradient selection methods over a mixing time of 12 h. The resonance signal at 4.700 ppm (TMS) was used as an internal reference.

2.4. Determination of the association constant

The association constants (Ka values) of $\beta CDNH_2$@4CPA, $\beta CDNH_2$@4ABA and $\beta CDNH_2$@PhEA complexes in water were obtained using the phase solubility method (Connors, 1997; Higuchi & Connors, 1965). The measurements were conducted using a V-760 JASCO UV spectrophotometer (see Supplementary Material, S3).

2.5. Preparation of substrates modified with the per-(6-amino-6-deoxy)-β-CD monolayer

Silicon wafers (100) were cut to 1.5 cm × 1.7 cm. The small silicon wafers were immersed in a boiling solution of NH_3:H_2O_2:H_2O (1:1:5) at 70 °C for 45 min to obtain an external oxide layer with a thickness of 1 nm and an additional native oxide layer. The silicon wafers were rinsed 3 times with water and dried under a N_2 stream.

Substrate functionalization was performed following the method described by Onclin et al. (2004), with modifications. After forming the oxidized surfaces, the silicon wafers were immersed in a 2 % APTES solution in toluene at 70 °C for 20 s. Finally, the substrates were rinsed copiously with toluene and dried under a stream of N_2.

The incorporation of isothiocyanate-terminated layers using a DITC solution and the subsequent incorporation of the $\beta CDNH_2$ solution for the formation of $\beta CDNH_2$M was performed as previously described (Onclin et al., 2004).

$\beta CDNH_2$ was synthesized following the procedure described by Ashton, Königer, Stoddart, Alker, and Harding (1996)) (see Supplementary Material, S1).

2.6. Characterization of substrates modified with the per-(6-amino-6-deoxy)-β-CD monolayer

2.6.1. Ellipsometric measurements

Using a vertical computer-controlled DRE-EL02 system (Ratzeburg, Germany) in a room conditioned at 24 ± 1 °C, ellipsometric measurements were performed. The incidence angle (φ) was set to 70.0° using a laser at a wavelength of 632.8 nm. A multilayer model based on the Jones matrix calculation for the interpretation of ellipsometric data was used (Silva, Urzúa, Petri, & Dubin, 2010). The expected thickness for each monolayer was determined using ChemDraw software, version 15 (Perkin Elmer).

The thickness of the SiO_2 layers was determined considering a Si refractive index of n = 3.858 ± 0.0180 and infinite thickness in contact with air (n = 1.00). The refractive index used for each subsequent stage was n = 1.462 for SiO_2, n = 1.424 for APTES and n = 1.5 for DITC and $\beta CDNH_2$ (Palik, 1985). The results correspond to an average of the measurements from 100 to 200 samples.

2.6.2. Contact angle

The measurements were performed using a home-built apparatus that included a digital camera connected to a computer. Water droplets with volumes of 8 and 4 μL were used for the advancing angle (θa) and receding angle (θr), respectively. The reported data are the average of fifteen samples for each stage.

2.6.3. X-ray photoelectronic spectroscopy

A Perkin Elmer PHI 1257 scanning Auger microscope with a UHV chamber, a hemispherical electron energy analyser, and an X-ray source from the Kα radiation of an Al anode (hν = 1486.6 eV) was used. During data acquisition, the pressure in the main chamber was maintained at 10^{-7} Pa. The link energy scale was calibrated using a carbon signal at 284.6 eV, with an accuracy of 70.1 eV.

2.6.4. Atomic force microscopy

Topographic images and surface roughness measurements were obtained by atomic force microscopy (AFM, Omicron) in tapping mode

at room temperature under high-vacuum conditions. Silicon tips (AC240TS-R3, Asylum Research) were used with a resonance frequency of 70 kHz and a constant spring of 2 N/m (see Supplementary Material, S4)

2.7. Sorption of pollutants and reusability of the modified substrate

Pollutant sorption assays were performed at room temperature and neutral pH. These studies were conducted by immersing six modified substrates in a 0.1 mmol/L initial solution. The variation in their concentration was recorded in the supernatant solution from 0 to 168 h using a V-760 JASCO UV spectrophotometer (see Supplementary Material, S5).

Reusability tests of the modified substrate were performed by immersion in a 0.1 mmol/L 4CPA solution. After each assay, the substrates were rinsed with ethanol and left in an ultrasonic bath for 5 min to eliminate the included contaminant.

3. Results and discussion

3.1. Characterization of the new inclusion complexes in solution

The βCDNH$_2$@4CPA, βCDNH$_2$@4ABA and βCDNH$_2$@PhEA complexes were characterized in solution using ^{1}H-NMR and ROESY spectroscopy. ^{1}H-NMR was used to measure the complexation shifts, i.e., the difference between the free and complexed resonance frequency (in ppm) for the same nucleus. ROESY was used to elucidate the arrangement of guest molecules within the matrix (Schneider, Hacket, Rüdiger, & Ikeda, 1998).

Fig. 1 shows the full ^{1}H-NMR spectra of the βCDNH$_2$ inclusion complexes with organic pollutants and the respective proton assignments.

Proton chemical shifts for the individual species and in the inclusion complexes are shown below. Table 1 corresponds to the pollutants, and Table 2 corresponds to βCDNH$_2$.

The NMR study of complexes βCDNH$_2$@4CPA and βCDNH$_2$@4ABA shows chemical shifts of the aromatic protons of the both guest molecules to higher fields, probably due to the spatial restriction when these molecules are included in the matrix, generating an effect of shielding of their atomic nuclei. For the βCDNH$_2$@PhEA complex, the protons of the aromatic ring and ethyl chain are shifted towards lower fields, probably because the PhEA molecule is displaced towards the narrow matrix edge where the NH$_2$ groups are located, which are electron density acceptors. This phenomenon is observed with higher intensity for the protons of the ethyl chain.

For the three inclusion complexes, there is a noticeable chemical shift in the signals from the H3 and H5 protons of βCDNH$_2$, mainly due to the inclusion of the contaminant molecules. The displacement to a high or low field is due to the degree of interaction between the matrix and the respective guest and the orientation they adopt within the matrix cavity. This observation is better clarified in two-dimensional resonance studies (see Fig. 2).

When analysing the integrals of the signals for the βCDNH$_2$@4CPA, βCDNH$_2$@4ABA and βCDNH$_2$@PhEA complexes, a 1:1 stoichiometry (matrix:guest) was established (see Supplementary Material, S2.1).

Through ROESY, it was possible to determine the preferential orientation that the guest molecules adopt inside the βCDNH$_2$ cavity. Fig. 2(a)-(c) shows the cross-peaks for the proton signals of greatest interest for studying the interactions between each guest molecule and βCDNH$_2$. A strong correlation between the aromatic proton signals of the guest molecules with the H3 and H5 protons of βCDNH$_2$ demonstrates the inclusion of the aromatic rings. Complementary cross-peak sections in the ROESY spectra are shown in the Supplementary Material S2.2, which supports the proposed inclusion geometry for the βCDNH$_2$@4CPA, βCDNH$_2$@4ABA and βCDNH$_2$@PhEA complexes.

βCD inclusion complexes with an average Ka of 490 Lmol^{-1} have been reported (Rao & Stella, 2003). Similar values for some pollutants and molecules containing aromatic rings have been observed (2017, Asela et al., 2017; Flaherty et al., 2013; Sierpe et al., 2015). In this study, the values of Ka for the βCDNH$_2$@4CPA, βCDNH$_2$@PhEA and βCDNH$_2$@4ABA complexes were 601, 491 and 40 Lmol^{-1}, respectively (see Supplementary Material, S3). Higher values of Ka could indicate that the pollutants would be more difficult to remove from the substrate. However, the values reported for the three complexes support the idea that matrices with βCDNH$_2$M could be used as a strategy of environmental remediation.

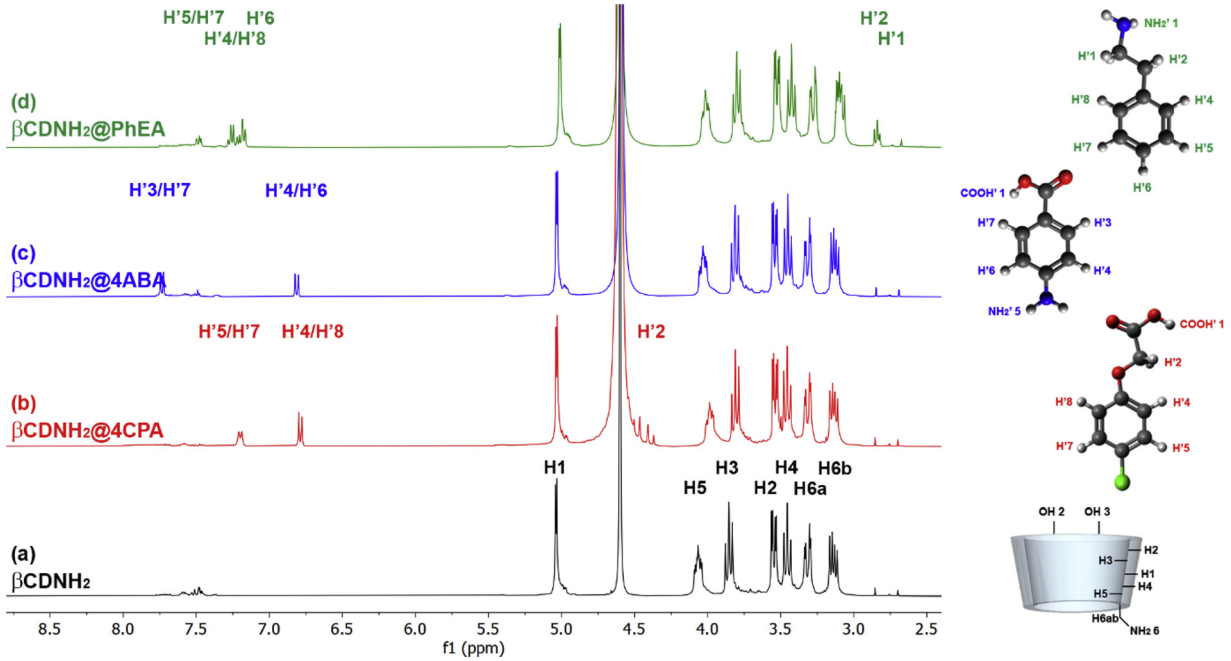

Fig. 1. ^{1}H-NMR spectra (7.0 mmol/L in D$_2$O) of (a) βCDNH$_2$, (b) βCDNH$_2$@4CPA, (c) βCDNH$_2$@4ABA and (d) βCDNH$_2$@PhEA complexes with the proton assignments for all species.

Table 1
^{1}H-NMR chemical shifts of the individual pollutants and in their respective inclusion complexes.

βCDNH$_2$@4CPA complex				βCDNH$_2$@4ABA complex				βCDNH$_2$@PhEA complex			
H assignments	δ 4CPA (ppm)	δ complex (ppm)	Δδ (ppm)	H assignments	δ 4ABA (ppm)	δ complex (ppm)	Δδ (ppm)	H assignments	δ PhEA (ppm)	δ complex (ppm)	Δδ (ppm)
H'2	4.607	4.531	−0.076	H'3/H'7	7.788	7.844	0.144	H'1	2.800	3.165	0.365
H'4/H'8	6.900	6.881	−0.019	H'4/H'6	6.848	6.922	0.056	H'2	2.686	2.942	0.256
H'5/H'7	7.299	7.292	−0.007					H'4/H'8	7.238	7.274	0.036
								H'5/H'7	7.320	7.364	0.044
								H'6	7.214	7.312	0.098

3.2. Step-by-step characterization of the solid substrate modified with per-(6-amino-6-deoxy)-β-CD

The surface modification stages were i) amino-terminated monolayer formation, ii) isothiocyanate-terminated monolayer formation, and iii) βCDNH$_2$ incorporation (see Fig. 3). Each stage was monitored by ellipsometry, contact angle, XPS, and AFM. The results obtained by ellipsometry and contact angle are shown in Table 3.

The SiO_2 average thickness was 1.0 ± 0.1 nm for more than 200 samples measured. For APTES monolayers, the average thickness was 0.80 ± 0.05 nm, which corresponds to the expected thickness of the APTES monolayer in a stretched and perpendicular conformation on the surface. The contact angles of 61° for the advance angle and 28° for the receding angle are in agreement with previously reported values, but they are lower than expected for an -NH_2 terminal surface. This could be related to the hydration of the surface caused by environmental humidity, transforming the amino-terminal groups into -NH_3^+ and increasing the hydrophilic properties of the surface (Pasternack, Amy, & Chabal, 2008).

For the DITC monolayer, the optimum thickness should be approximately 1.1 nm, assuming an extended conformation. However, an average thickness of 0.60 nm was obtained. Therefore, a molecular inclination angle of 33° was predicted. The increase in the advance and receding angles after the incorporation of the DITC monolayer correlates with the findings described by Manning, Leigh, Ramos, Preece, and Eritja (2010)), which attribute this increase to greater surface hydrophobicity.

Finally, βCDNH$_2$ was incorporated for βCDM formation. The pH must be adjusted with an ammonia solution since the addition of a sodium hydroxide solution could favour the reduction of the -NCS terminal group to an -NH_2 group, which prevents thioamide bond formation (Lee, Guivarch, Van Dau, Tessier, & Krstulovic, 2003).

Table 3 shows a decrease in the contact angle values for βCDM as the surface becomes hydrophilic since the secondary hydroxyl groups of the βCD molecules are exposed to the surface. The thickness determined was 0.93 nm, which coincides with the length reported for the βCD unit, evidencing monolayer formation (Del Valle, 2004; Onclin et al., 2004).

To characterize the chemical composition and electronic state in each stage, XPS measurements were performed. Fig. 4(a) shows the acquired full spectra, which were normalized according to the Si2p peak. The intensity increases in the characteristic C1s, O1s, S2p and N1s peaks indicate the stacking of each molecular monolayer on the surface up to the final formation of βCDNH$_2$M. The analysis performed on the oxide surface detected the presence of silicon, oxygen and carbon, where the presence of carbon can be attributed to the XPS source. In the following stages, the appearance of C, N and S signals is concordant with the expected composition for the incorporated molecular monolayers.

Fig. 4(b) corresponds to the curve fittings of each characteristic peak. In the first stage of the silicon wafer oxidation process, the characteristic Si2p peaks are observed. The lower binding energy at 99.2 eV is associated with Si° from the bulk silicon wafer, the binding energy at 100.4 eV corresponds to Si^{1+}, and the higher binding energy at 103.2 eV corresponds to Si^{4+} from silicon dioxide (Araya et al., 2012; Flores, Fuenzalida, & Häberle, 2005).

In the XPS spectrum for the C1s peak, a change in the characteristic peak during modification was observed (Fig. 4). The most intense peak corresponded to the C—C bonds, which appeared at a binding energy of 284.6 eV when the APTES monolayer was incorporated; this peak increased to 284.8 eV in the subsequent substrate modifications. A second peak was identified at 285.8 eV, which was assigned to C—N bonds, and their binding energies increased to 286.0 eV and 286.4 eV when monolayers of DITC and βCDNH$_2$ were incorporated, respectively. A third peak of lower intensity appeared at 288.0 eV in the APTES monolayer formation and was attributed to C—O bonds (Thangaraju, Karthikeyan, Prakash, Babu, & Hayakawa, 2015). Then, this signal slightly increased its binding energy to 288.2 eV, which could be attributed to the additional presence of thioamide bonds when the DITC and βCDNH$_2$ monolayers were incorporated (Zhang, Zhou, Ding, Fu, & Wang, 2017).

The curve fittings for the O1s peak show a peak of greater intensity at 532.4 eV, which can be attributed mainly to silicon oxide. Finally, the incorporation of βCDNH$_2$M was confirmed by the presence of a peak at 533.4 eV, which was attributable to cyclic C—O—C bonds (Beanson & Briggs, 1992).

The characteristic N1s peak at approximately 400.0 eV consisted of three distinct peaks at 398 eV, 400 eV and 402 eV, which can be

Table 2
^{1}H-NMR chemical shifts of βCDNH$_2$ in its free state and in the respective inclusion complexes.

H assignments	Pure βCDNH$_2$	βCDNH$_2$@4CPA complex		βCDNH$_2$@4ABA complex		βCDNH$_2$@PhEA complex	
	δ βCDNH$_2$ (ppm)	δ complex (ppm)	Δδ (ppm)	δ complex(ppm)	Δδ (ppm)	δ complex(ppm)	Δδ (ppm)
H1	5.138	5.128	−0.010	5.143	−0.005	5.112	−0.026
H2	3.648	3.634	−0.014	3.652	0.004	3.626	−0.022
H3	3.955	3.905	−0.050	3.923	−0.032	3.901	−0.054
H4	3.556	3.550	−0.006	3.560	0.004	3.526	−0.030
H5	4.167	4.081	0.086	4.142	−0.025	4.116	−0.051
H6a	3.416	3.410	−0.006	3.424	0.008	3.378	−0.038
H6b	3.240	3.232	−0.008	3.240	0.000	3.198	−0.042

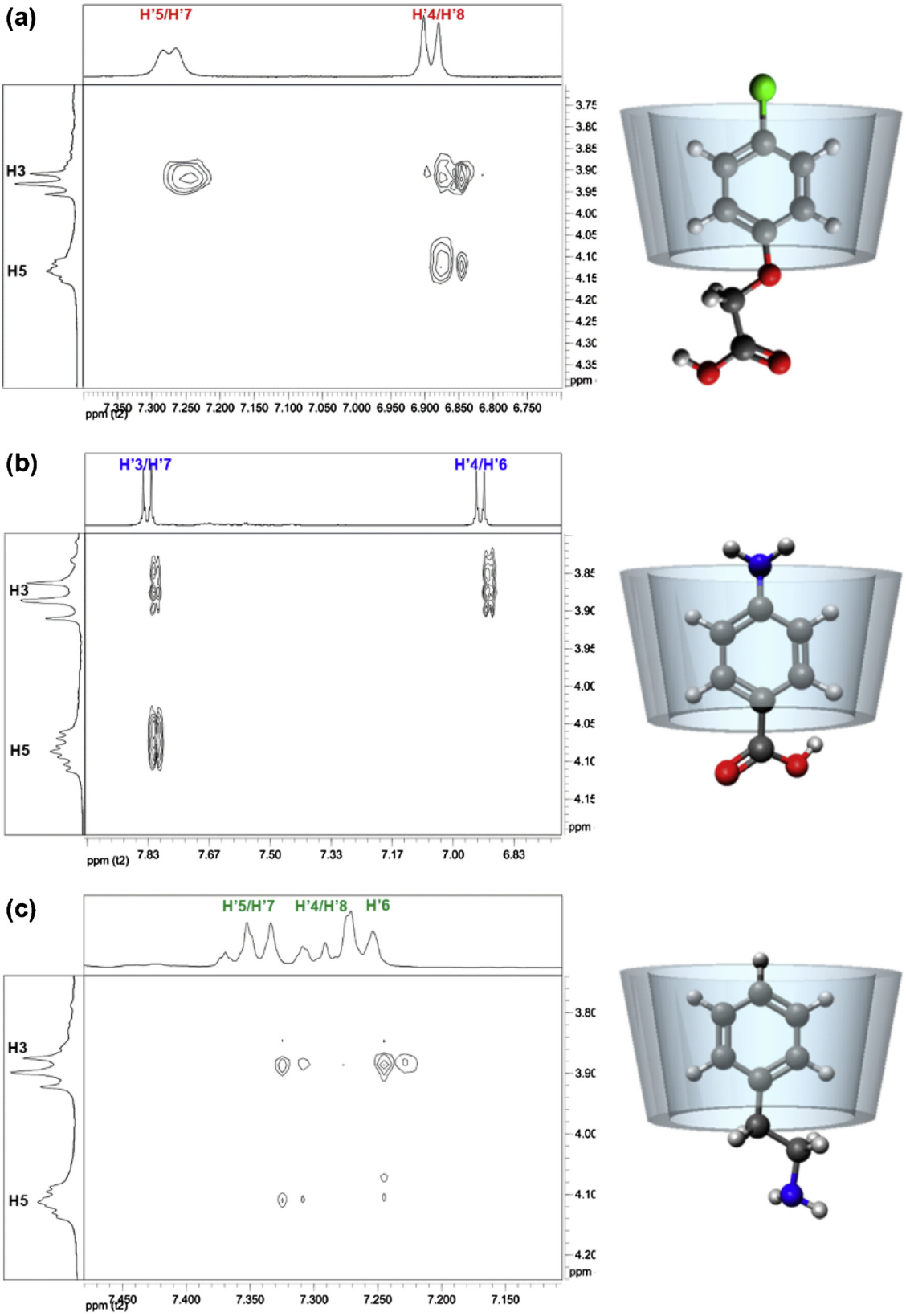

Fig. 2. Cross-peaks in the ROESY spectra for the aromatic protons of the guest molecules with the H3 and H5 protons of $\beta CDNH_2$ and the proposed inclusion geometry for the a) $\beta CDNH_2$@4CPA, b) $\beta CDNH_2$@4ABA and c) $\beta CDNH_2$@PhEA complexes.

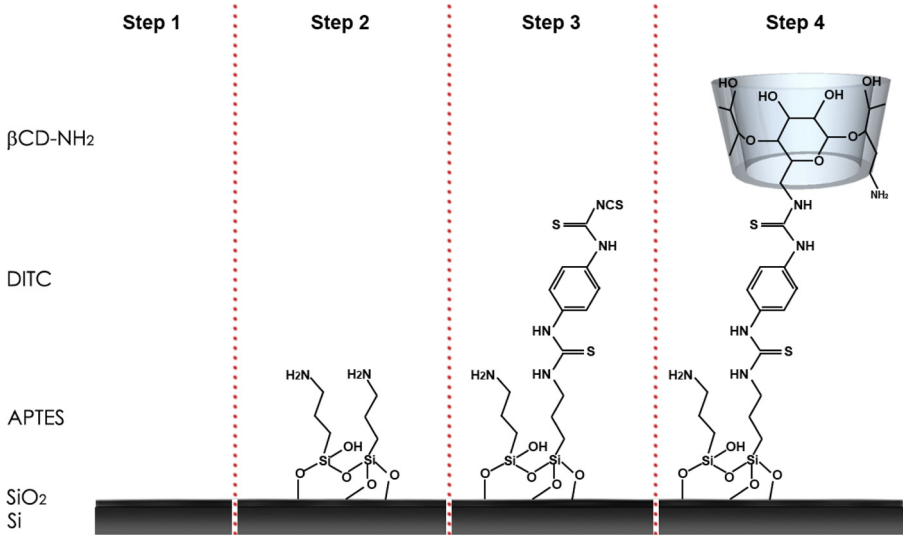

Fig. 3. Schematic representation of the $\beta CDNH_2M$ preparation on silicon surfaces.

Table 3
Ellipsometric and contact angle measurements for each monolayer.

Monolayer	θ_a (°)	θ_r (°)	Experimental ellipsometric thickness (nm)	Expected thickness (nm)
-NH_2	61 ± 1	28 ± 2	0.80 ± 0.05	0.80
-NCS	64 ± 2	38 ± 3	0.60 ± 0.10	1.10
-βCD	49 ± 1	27 ± 2	0.93 ± 0.02	0.79

assigned to the -NH_2 group, N—C bonds and NH_3^+ group, respectively. The signal broadening and increase in the binding energy of the peak at 400 eV when the monolayers of DITC and $\beta CDNH_2$ were incorporated can be attributed to the formation of thioamide bonds (Graf et al., 2010; Tischer et al., 2012).

The doublet signal characteristic of S2p, which appeared at 168 eV, confirms the presence of sulfur in the thioamide bond formed after the incorporation of the molecular monolayer of DITC (Tischer et al., 2012; Zhang et al., 2017). The signals found at 162 eV and 170 eV corresponded to the presence of a S species with sp^2 hybridization and to interactions between nearby sulfur atoms, respectively (Beanson & Briggs, 1992; Graf et al., 2010).

Fig. 5 presents topographic AFM images representative of surfaces with SiO_2, APTES, DITC and $\beta CDNH_2$ monolayers. These monolayers have homogeneous topography with regular morphologies and root-mean-square (RMS) roughness ranging between 0.2 and 0.5 nm for all stages (see Supplementary Material, S4). These micrographs complement the results obtained by ellipsometry, corroborating the preparation of ordered and densely packed monolayers in each of the stages.

3.3. Uptake assays of the pollutants and regeneration tests of the modified substrates

The sorption capacity of the substrates in each assay was calculated according to Eq. (1):

$$q_t = \frac{(C_0 - C_t) \times V}{n} \quad (1)$$

where C_0 and C_t are the concentrations at time = 0 and t, respectively; V is the volume of the respective pollutant solution; and n is the number of substrates used in each experiment. The sorption capacity at equilibrium, q_e, was determined using an analogous equation, considering the equilibrium concentration, C_e. Fig. 6 shows the increasing sorption capacity of each pollutant over time until equilibrium conditions were obtained.

The sorption kinetics were investigated using two kinetic models, comprising pseudo-first order (2) and pseudo-second order (3) equations, expressed as:

$$\ln(q_e - q_t) = ln(q_e) - k_1 t \quad (2)$$

$$\frac{t}{q_t} = \frac{1}{k_2 q_e^2} + \frac{t}{q_e} \quad (3)$$

where k_1 and k_2 are the pseudo-first and pseudo-second order velocity constants, respectively, and q_e and q_t are the sorption capacities (mmol/substrate) at equilibrium and at time t, respectively. Applying the pseudo-first order kinetic model, the values of k_1 and q_e can be calculated from the slope and the intercept of the line $\ln(q_e - q_t)$ plotted against t. Likewise, k_2 and q_e can be determined from the intercept and slope of the line t/q_t plotted against t for the pseudo-second order model (Aly, Graulet, Scales, & Hanley, 2014; Ho & McKay, 1999).

The three pollutants show similar sorption behaviours with two sections of different slopes, as displayed in Fig. 6. The contact times in the first section vary between 0 and 6 h for 4ABA and 0 – 10 h for PhEA and 4CPA. The graph shows that the slope of the first section, depending on the sorbate, has values between 14 and 21 times larger than the second section before reaching equilibrium conditions (see Supplementary Material, S5). Finally, a plateau was observed after 144 h for 4ABA and 120 h for PhEA and 4CPA, which suggests that the sorption capacity of the pollutants in equilibrium has been reached (Fig. 6).

Pseudo-first order kinetics are associated with an adsorption (physisorption) process, and pseudo-second order corresponds to an absorption process (chemisorption) (Zou et al., 2016). The results obtained by applying the two kinetic models over time until reaching the sorption capacity at equilibrium show that a linear fit for the pseudo-second order kinetic behaviour is adequate (see Supplementary Material, S5). The adsorption and absorption processes could occur simultaneously. Physisorption is favoured by surface hydration due to the hydrophilic nature of the substrates functionalized with $\beta CDNH_2M$, improving the interaction with pollutant molecules dissolved in water. The substrate can continue to capture pollutant molecules through inclusion in the cavities of modified βCD after its accumulation on the surface.

Table 4 shows the results obtained by applying the kinetic models for 4CPA sorption; the results for 4ABA and PhEA sorption are shown in the Supplementary Material, S5. The highest values of R^2 and the best coincidence between the experimental and determined q_e values confirm pseudo-second-order kinetic behaviour. The second-order model

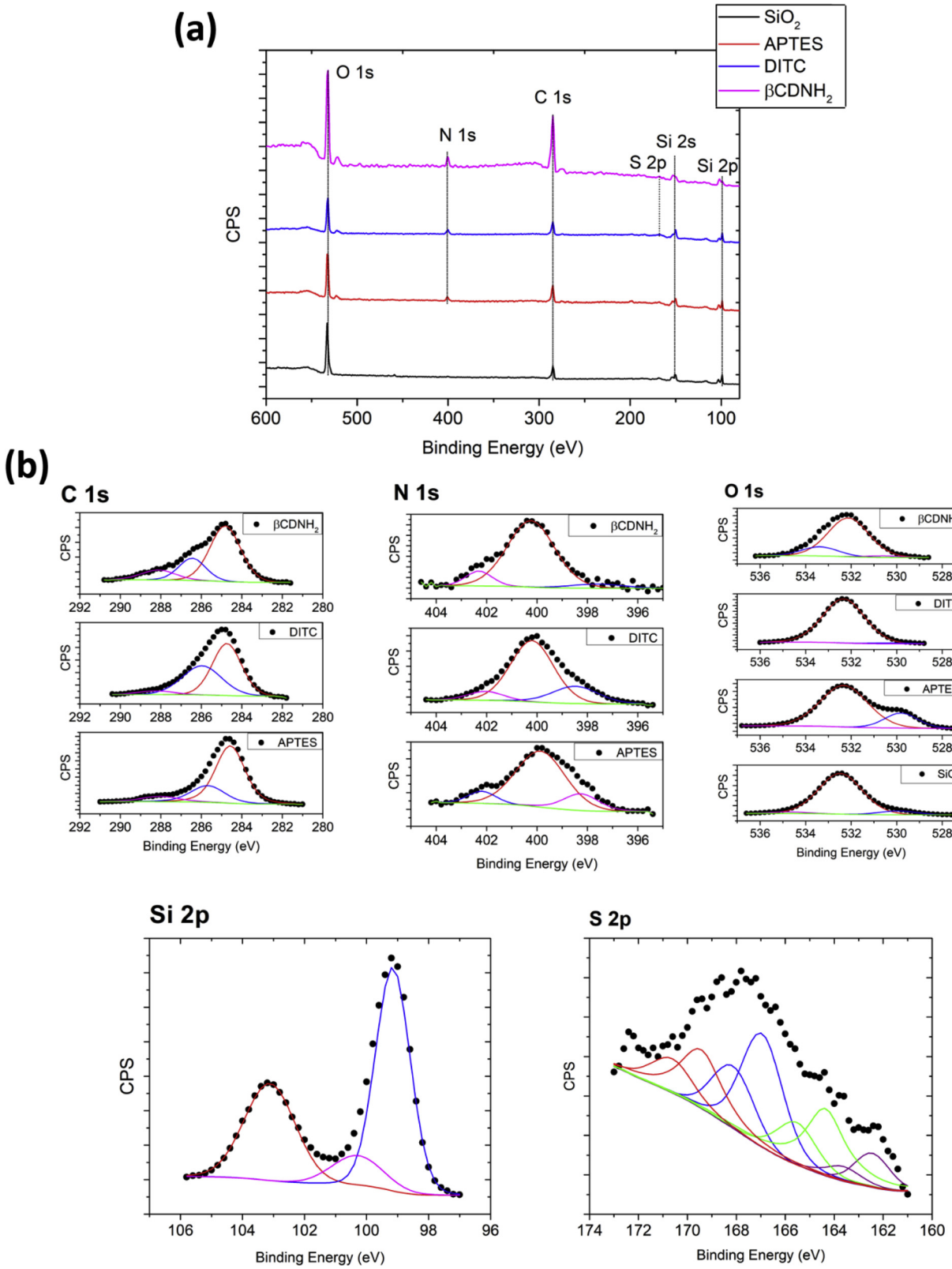

Fig. 4. (a) Full XPS spectra acquired during all modification stages. (b) Curve fittings of each characteristic peak in the XPS spectra.

suggests that the rate-limiting step may be a supramolecular inclusion process, demonstrating that the pollutant sorption behaviour on the substrates modified with $\beta CDNH_2M$ is dominated by matrix-guest interactions (Triki, Tanazefti, & Kochkar, 2017; Yang et al., 2013; Zou et al., 2016).

Table 4 shows a 4CPA experimental sorption capacity at equilibrium of 4413×10^{-5} mmol/substrate; this value is 50.76 % higher than the capture capacity of the unmodified substrate (see Supplementary Material, S5.1).

Additionally, the presence of included 4CPA was corroborated by

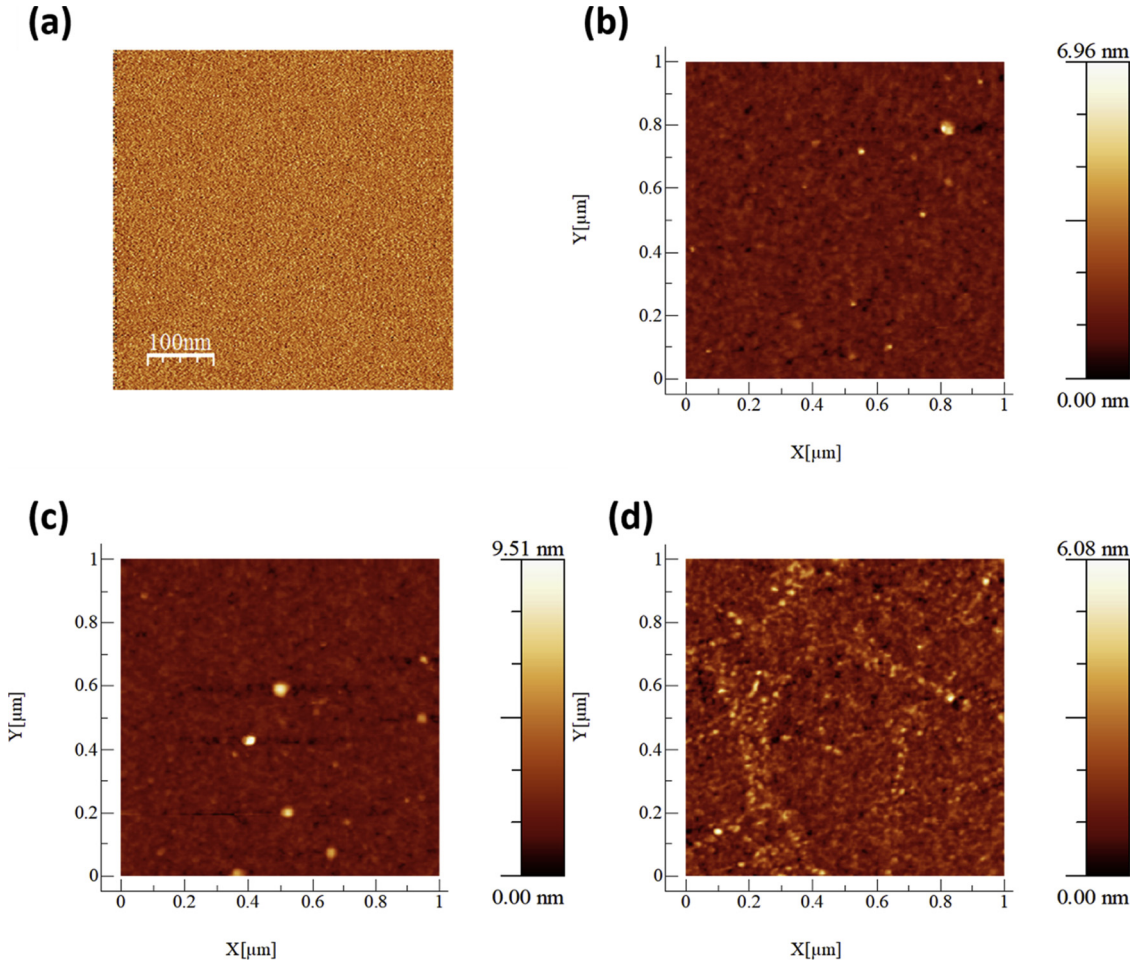

Fig. 5. AFM micrographs of (a) an SiO_2 surface, and monolayers terminated in (b) -NH_2 (APTES), (c) -NCS (DITC), and (d) βCDNH_2.

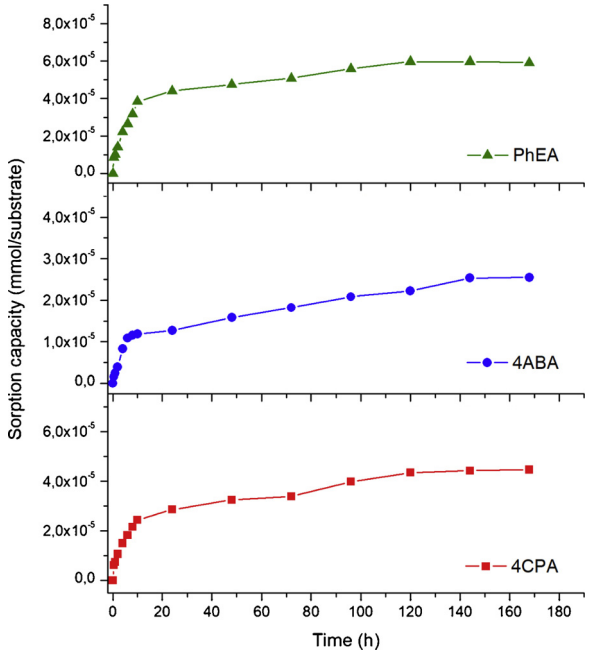

Fig. 6. Sorption capacity over time in contact with (a) 4CPA, (b) 4ABA and (c) PhEA in aqueous solution.

Table 4
Summary of results obtained from the kinetic models applied to 4CPA capture.

Kinetic model	q_e (exp.) [mmol/substrate]	q_e (calc.) [mmol/substrate]	k_1 [h^{-1}]	R^2
Pseudo-first order	4.413×10^{-5}	3.513×10^{-5}	$2{,}662 \times 10^{-2}$	0.892
Kinetic model	q_e (exp.) [mmol/substrate]	q_e (calc.) [mmol/substrate]	k_2[substrate/(mmol*h)]	R^2
Pseudo-second order	4.413×10^{-5}	4.238×10^{-5}	$3{,}359 \times 10^{3}$	0.980

XPS measurements (see Supplementary Material, S6).

Fig. 7 shows the reusability results for the capture of 4CPA after four consecutive regeneration cycles measured every 24 h. The graph shows that the substrates can operate with more than 90 % efficiency, with 100 % sorption capacity considered the maximum amount adsorbed until 24 h. This is similar to other reported results on βCD-based sorbent materials. This substrate does not leave a residue because it is a compact material that can be easily removed from a water matrix (Alzate-Sánchez, Smith, Alsbaiee, Hinestroza, & Dichtel, 2016; Flaherty et al., 2013; Schofield et al., 2012).

4. Conclusions

Silicon wafers functionalized with βCDNH_2M were prepared successfully, yielding stable, robust and homogeneous material for the

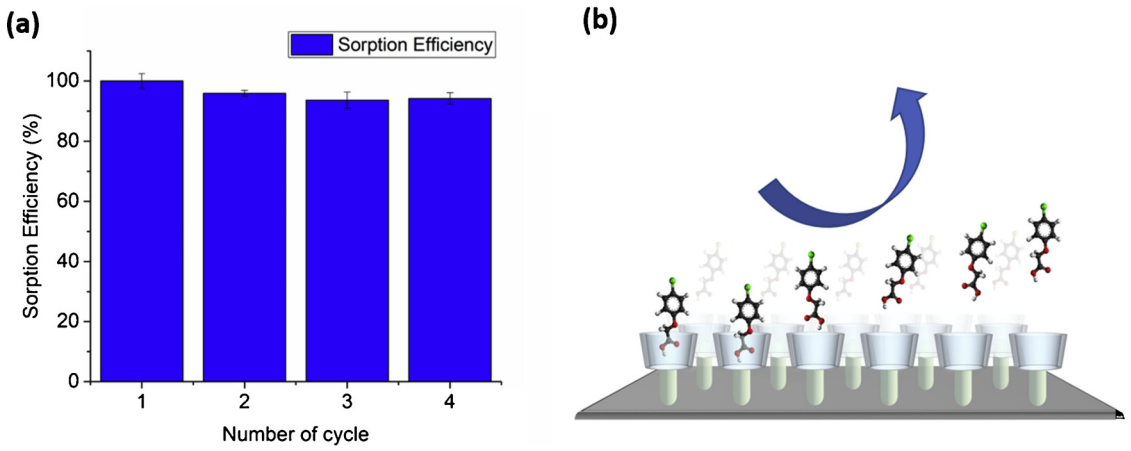

Fig. 7. (a) Graphical representation of the reusability test for 4CPA capture. (b) Schematic representation of 4CPA release after each cycle.

sorption of pollutants. The sorption capacity of this solid was evaluated by performing assays with three potential pollutants: 4-chlorophenoxyacetic acid, 4-aminobenzoic acid and phenylethylamine. This substrate showed a high sorption capacity at equilibrium between 2.5×10^{-5} and 6.0×10^{-5} mmol/substrate for the studied pollutants. This surface can be reused four times with an efficiency equal to the initial efficiency, being a versatile platform for the capture of other organic pollutants from water and leaving no residue. Our studies show that the kinetic behaviour in the sorption of pollutants conforms to a pseudo-second order model, coinciding with the results obtained for other sorbent βCD-based materials.

Author contributions

Nicolás I Yutronic: Group leader, research design, Contribute research funds, analysis and discussion of results.

Bárbara A. Herrera: Postdoctoral researcher, design and carrying out of experiments, bibliographic review, manuscript and figure writing, analysis and discussion of results.

Marcela del P. Urzúa: Funding, ellipsometry measurements and contact angles.

Erika P. Lang: NMR measurement and analysis.

Marcos I. Flores: Measurement and analysis of XPS and AFM.

Rodrigo A. Sierpe: interpretation and analysis of results, design and construction of figures.

Tamara C. Bruna: Synthesis of systems and development of experiments, literature review.

Paul S. Jara: research design; contribute research funds, analysis and discussion of results and manuscript writing.

Acknowledgements

The authors thank the funding granted by FONDECYT for projects No 3140485, 3180706, 1160114, 1171611 and 1151221, Projects PIA Anillo ACT-1412 and Millennium Nucleus Multifunctional Material for Surface Science Applications. T. Bruna thanks CONICYT for doctoral fellowship No 21120856.

Appendix A. Supplementary data

Supplementary material related to this article can be found, in the online version, at doi:https://doi.org/10.1016/j.carbpol.2020.115865.

References

Ahmad, T., Rafatullah, M., Ghazali, A., Sulaiman, O., Hashim, R., & Ahmad, A. (2010). Removal of pesticides from water and wastewater by different adsorbents: A review. *Journal of Environmental Science and Health, Part C, 28*, 231–271.

Aly, Z., Graulet, A., Scales, N., & Hanley, T. (2014). Removal of aluminium from aqueous solutions using PAN-based adsorbents: Characterisation, kinetics, equilibrium and thermodynamic studies. *Environmental Science and Pollution Research, 21*, 3972–3986.

Alzate-Sánchez, D. M., Smith, B. J., Alsbaiee, A., Hinestroza, J. P., & Dichtel, W. R. (2016). Cotton fabric functionalized with a β-cyclodextrin polymer captures organic pollutants from contaminated air and water. *Chemistry of Materials, 28*, 8340–8346.

Araya, M., Díaz-Droguett, D. E., Ribeiro, M., Albertin, K. F., Avila, J., Fuenzalida, V. M., et al. (2012). Photoluminescence in silicon/silicon oxide films produced by the pulsed electron beam ablation technique. *Journal of Non-Crystalline Solids, 358*, 880–884.

Asela, I., Noyong, M., Simon, U., Andrades-Lagos, J., Campanini-Salinas, J., Vásquez-Velásquez, D., et al. (2017). Gold nanoparticles stabilized with βcyclodextrin-2-amino-4-(4-chlorophenyl)thiazole complex: A novel system for drug transport. *PloS One, 12*, e0185652.

Ashton, P. R., Königer, R., Stoddart, J. F., Alker, D., & Harding, V. D. (1996). Amino acid derivatives of β-cyclodextrin. *The Journal of Organic Chemistry, 61*, 903–908.

Awad, A. M., Shaikh, S. M. R., Jalab, R., Gulied, M. H., Nasser, M. S., Benamor, A., et al. (2019). Adsorption of organic pollutants by natural and modified clays: A comprehensive review. *Separation and Purification Technology, 228*, 115719.

Beanson, G., & Briggs, D. (1992). *High resolution XPS of organic polymers: The scienta ESCA 300 database.* Chichester: Wiley Interscience.

Connors, K. A. (1997). The stability of cyclodextrin complexes in solution. *Chemical Reviews, 97*, 1325–1358.

Crini, G. (2014). Review: A history of cyclodextrins. *Chemical Reviews, 114*, 10940–10975.

Del Valle, E. M. M. (2004). Cyclodextrins and their uses: A review. *Process Biochemistry, 39*, 1033–1046.

Derylo-Marczewska, A., Blachnio, M., Marczewski, A. W., Swiatkowski, A., & Buczek, B. (2017). Adsorption of chlorophenoxy pesticides on activated carbon with gradually removed external particle layers. *Chemical Engineering Journal, 308*, 408–418.

Flaherty, R. J., Nshime, B., DeLaMarre, M., DeJong, S., Scott, P., & Lantz, A. W. (2013). Cyclodextrins as complexation and extraction agents for pesticides from contaminated soil. *Chemosphere, 91*, 912–920.

Flores, M., Fuenzalida, V., & Häberle, P. (2005). Thermal effects in the size distribution of SiC nanodots on Si(111). *Physica Status Solidi, 202*, 1959–1966.

Geissen, V., Mol, H., Klumpp, E., Umlauf, G., Nadal, M., van der Ploeg, M., et al. (2015). Emerging pollutants in the environment: A challenge for water resource management. *International Soil and Water Conservation Research, 3*, 57–65.

Graf, N., Lippitz, A., Gross, T., Pippig, F., Holländer, A., & Unger, W. E. S. (2010). Determination of accessible amino groups on surfaces by chemical derivatization with 3,5-bis(trifluoromethyl)phenyl isothiocyanate and XPS/NEXAFS analysis. *Analytical and Bioanalytical Chemistry, 396*, 725–738.

Halberstadt, A. L., van der Zee, J. V. F., Chatha, M., Geyer, M. A., & Powell, S. B. (2019). Chronic treatment with a metabotropic mGlu2/3 receptor agonist diminishes behavioral response to a phenethylamine hallucinogen. *Psychopharmacology, 236*, 821–830.

Higuchi, T., & Connors, K. A. (1965). Phase solubility techniques. In C. N. Reilly (Ed.). *Advances in analytical chemistry and instrumentation* (pp. 117–212). New York, NY: Wiley-Interscience.

Ho, Y. S., & McKay, G. (1999). Pseudo-second order model for sorption processes. *Process Biochemistry, 34*, 451–465.

Ivshina, I., Tyumina, E., & Vikhareva, E. (2018). Biodegradation of emerging pollutants: Focus on pharmaceuticals. *Microbiology Australia, 39*, 117–122.

Lagrost, C., Alcaraz, G., Bergamini, J.-F., Fabre, B., & Serbanescu, I. (2007). Functionalization of silicon surfaces with Si–C linked β-cyclodextrin monolayers. *Chemical Communications, 10*, 1050–1052.

Lee, C. R., Guivarch, F., Van Dau, C. N., Tessier, D., & Krstulovic, A. M. (2003). Determination of polar alkylating agents as thiocyanate/isothiocyanate derivatives by reaction headspace gas chromatography. *The Analyst, 128*, 857–863.

Leopold, A. C., van Schaik, P., & Neal, M. (1960). Molecular structure and herbicide

adsorption. *Weeds, 8*, 48–54.
Ling, X. Y., Reinhoudt, D. N., & Huskens, J. (2008). Reversible attachment of nanostructures at molecular printboards through supramolecular glue. *Chemistry of Materials, 20*, 3574–3578.
Lu, P., Cheng, J., Li, Y., Li, L., Wang, Q., & He, C. (2019). Novel porous β-cyclodextrin/pillar[5]arene copolymer for rapid removal of organic pollutants from water. *Carbohydrate Polymers, 216*, 149–156.
Manning, B., Leigh, S. J., Ramos, R., Preece, J. A., & Eritja, R. (2010). Fabrication of patterned surfaces by photolithographic exposure of DNA hairpins carrying a novel photolabile group. *Journal of Experimental Nanoscience, 5*, 26–39.
Méndez-Torres, A. M., Sandoval-Altamirano, C., Sánchez-Arenillas, M., Marco, J. F., & Yáñez, C. (2018). Amino β-cyclodextrins immobilized on gold surfaces: Effect of substituents on host-guest interactions. *Electrochimica Acta, 282*, 860–869.
Morin-Crini, N., & Crini, G. (2013). Environmental applications of water-insoluble β-cyclodextrin–epichlorohydrin polymers. *Progress in Polymer Science, 38*, 344–368.
Naik, P., Abdellah, I. M., Abdel-Shakour, M., Acharaya, M., Pilicode, N., El-Shafei, A., et al. (2018). An efficient aniline-based co-sensitizer for high performance N3-sensitized solar cells. *ChemistrySelect, 3*, 12297–12302.
Niu, Y., Huang, T., Zhou, Z., Xu, G., Zhang, L., & Wei, T. (2015). Formation of cyclodextrin monolayer through a host–guest interaction with tailor-made phenyltriethoxysilane self-assembled monolayer. *Colloids and Surfaces A: Physicochemical and Engineering Aspects, 470*, 224–229.
Onclin, S., Mulder, A., Huskens, J., Ravoo, B. J., & Reinhoudt, D. N. (2004). Molecular printboards: Monolayers of β-cyclodextrins on silicon oxide surfaces. *Langmuir, 20*, 5460–5466.
Palik, E. D. (1985). *Handbook of optical constants of solids.* London, UK: Academic Press.
Pan, Y., Mu, N., Shao, S., Yang, L., Wang, W., Xie, X., et al. (2015). Selective surface acoustic wave-based organophosphorus sensor employing a host-guest self-assembly monolayer of β-cyclodextrin derivative. *Sensors, 15*, 17916–17925.
Pasternack, R. M., Amy, S. R., & Chabal, Y. J. (2008). Attachment of 3-(Aminopropyl) triethoxysilane on silicon oxide surfaces: Dependence on solution temperature. *Langmuir, 24*, 12963–12971.
Rao, V. M., & Stella, V. J. (2003). When can cyclodextrins be considered for solubilization purposes? *Journal of Pharmaceutical Sciences, 92*, 927–932.
Sabelli, H., Fink, P., Fawcett, J., & Tom, C. (1996). Sustained antidepressant effect of PEA replacement. *The Journal of Neuropsychiatry and Clinical Neurosciences, 8*, 168–171.
Salazar, S., Guerra, D., Yutronic, N., & Jara, P. (2018). Removal of aromatic chlorinated pesticides from aqueous solution using β-cyclodextrin polymers decorated with Fe_3O_4 nanoparticles. *Polymers, 10*, 1038–1057.
Schneider, H.-J., Hacket, F., Rüdiger, V., & Ikeda, H. (1998). NMR studies of cyclodextrins and cyclodextrin complexes. *Chemical Reviews, 98*, 1755–1786.
Schofield, W. C. E., Bain, C. D., & Badyal, J. P. S. (2012). Cyclodextrin-functionalized hierarchical porous architectures for high-throughput capture and release of organic pollutants from wastewater. *Chemistry of Materials, 24*, 1645–1653.
Sierpe, R., Lang, E., Jara, P., Guerrero, A. R., Chornik, B., Kogan, M. J., et al. (2015). Gold nanoparticles interacting with β-cyclodextrin–phenylethylamine inclusion complex: A ternary system for photothermal drug release. *ACS Applied Materials & Interfaces, 7*, 15177–15188.
Sierpe, R., Noyong, M., Simon, U., Aguayo, D., Huerta, J., Kogan, M. J., et al. (2017). Construction of 6-thioguanine and 6-mercaptopurine carriers based on βcyclodextrins and gold nanoparticles. *Carbohydrate Polymers, 177*, 22–31.
Silva, R. A., Urzúa, M. D., Petri, D. F. S., & Dubin, P. L. (2010). Protein adsorption onto polyelectrolyte layers: Effects of protein hydrophobicity and charge anisotropy. *Langmuir, 26*, 14032–14038.
Taka, A. L., Pillay, K., & Mbianda, X. Y. (2017). Nanosponge cyclodextrin polyurethanes and their modification with nanomaterials for the removal of pollutants from waste water: A review. *Carbohydrate Polymers, 159*, 94–107.
Thangaraju, D., Karthikeyan, R., Prakash, N., Babu, S. M., & Hayakawa, Y. (2015). Growth and optical properties of Cu_2ZnSnS_4 decorated reduced graphene oxide nanocomposites. *Dalton Transactions, 44*, 15031–15041.
Tischer, T., Goldmann, A. S., Linkert, K., Trouillet, V., Börner, H. G., & Barner-Kowollik, C. (2012). Modular ligation of thioamide functional peptides onto solid cellulose substrates. *Advanced Functional Materials, 22*, 3853–3864.
Triki, M., Tanazefti, H., & Kochkar, H. (2017). Design of β-cyclodextrin modified TiO_2 nanotubes for the adsorption of Cu(II): Isotherms and kinetics study. *Journal of Colloid and Interface Science, 493*, 77–84.
Wang, Y.-Y., Zhao, X.-L., Qian, H.-F., & Huang, W. (2018). Mono/double 3-methoxypropan-1-amine substituted pyridone azo dyes having isomeric ortho/para-aminobenzoic acids and corresponding methyl esters components. *Dyes and Pigments, 153*, 44–52.
Yang, S., Zong, P., Hu, J., Sheng, G., Wang, Q., & Wang, X. (2013). Fabrication of β-cyclodextrin conjugated magnetic HNT/iron oxide composite for high-efficient decontamination of U(VI). *Chemical Engineering Journal, 214*, 376–385.
Zhang, G., Zhou, Y., Ding, Z., Fu, L., & Wang, S. (2017). Nanosilica-supported thiosemicarbazide–glutaraldehyde polymer for selective Au(iii) removal from aqueous solution. *RSC Advances, 7*, 55215–55223.
Zou, Y., Wang, X., Ai, Y., Liu, Y., Ji, Y., Wang, H., et al. (2016). β-Cyclodextrin modified graphitic carbon nitride for the removal of pollutants from aqueous solution: Experimental and theoretical calculation study. *Journal of Materials Chemistry A, 4*, 14170–14179.